Plasma Chemistry and Plasma Processing (2022) 42:267–282
https://doi.org/10.1007/s11090-021-10223-1

ORIGINAL PAPER

Synergistic Effect of Co–Ni Bimetal on Plasma Catalytic Ammonia Synthesis

Y. Liu[1] · C.-W. Wang[1] · X.-F. Xu[1] · B.-W. Liu[1] · G.-M. Zhang[1] · Z.-W. Liu[1] · Q. Chen[1] · H.-B. Zhang[1]

Received: 10 August 2021 / Accepted: 9 December 2021 / Published online: 20 January 2022

Abstract
Plasma synthesis of ammonia is a potential and sustainable way of nitrogen fixation. In this work, a series of M/Al_2O_3 (M=Co, Ni, Co–Ni) catalysts have been investigated to enhance the synthesis of NH_3 from N_2 and H_2 in a dielectric barrier discharge (DBD) plasma reactor. Under the conditions of a volume ratio of N_2:H_2 of 1:1, a total gas flow rate of 200 mL min^{-1}, and a discharge temperature of 200 °C, the order of the ammonia synthesis rate filled with different catalysts was $Co–Ni/Al_2O_3 > Co/Al_2O_3 > Ni/Al_2O_3 > Al_2O_3 >$ only plasma. And the highest ammonia synthesis rate could be obtained was 1500 μmol g^{-1} h^{-1} by using $Co–Ni/Al_2O_3$ as the catalyst. Further research found that compared with single metal catalysis, on the one hand, the presence of Co–Ni bimetal reduced the total amount and strength of acidic sites on the catalyst surface, which is beneficial for the desorption of synthesized ammonia gas. On the other hand, the presence of Co–Ni bimetal enhanced the plasma discharge observed by the ICCD camera. At the same time, the electrical characterization was found changed with different catalysts added in the plasma synthesis process. Adding a Co–Ni bimetal loaded catalyst in the reaction system increased the average electric field (E) and improved the power efficiency.

Keywords Ammonia synthesis · Low temperature plasma · Packed-bed DBD reactor · Catalyst · Synthesis rate

Introduction

Ammonia (NH_3), as the world's second most produced chemical, is an important raw material for the production of many organic and inorganic materials (including fertilizers, plastics, resins, synthetic fibers, etc.) [1, 2]. 85% of them are used to make fertilizer. In addition, ammonia has the characteristics of high hydrogen content, high energy density and easy storage. It has great potential in energy storage [3–5] and used as hydrogen fuel [6–8], and will become an extremely important sustainable energy source in the future.

✉ H.-B. Zhang
hbzhang@bigc.edu.cn

[1] Laboratory of Plasma Physics and Materials, Beijing Institute of Graphic Communication, Beijing 102600, People's Republic of China

At present, the industrial synthesis of ammonia adopts the Haber–Bosch method. This traditional method of ammonia synthesis needs to be combined with highly active catalysts to convert nitrogen and hydrogen into ammonia under harsh conditions of 450–600 ℃ and 150–300 bar [9], which emits more than 300 million tons of carbon dioxide per year and high energy consumption. Its main raw material, fossil fuel, is a non-renewable resource, accounting for 1–2% of the world's total energy supply, ranking first in the chemical industry, which has a huge impact on the environment and economic development, and restricts the development of conventional ammonia synthesis process [10–13]. Therefore, it is expected to develop a green, effective, and economically sustainable method for small-scale distributed ammonia production to replace the Haber–Bosch process [14, 15]. In recent years, many researchers have devoted themselves to the direct synthesis of NH_3 from N_2 and H_2 through non-thermal plasma (NTP) technology under environmental conditions [16, 17]. NTP discharge generates high-energy electrons and active species (such as free radicals, excited atoms, molecules and ions), can be used to intensify the general chemical reaction which is not easy to happen at room temperature and atmospheric pressure. The application of plasma technology to synthesize ammonia has great potential for development.

Dielectric barrier discharge (DBD) technology is the most widely used technology in the plasma synthesis of NH_3 [18–20]. It has been widely applied to the generation of ozone [21], removal of gas pollutants [22–24], CH_4 activation [25, 26], CO_2 hydrogenation [27, 28] and the conversion of water gas and other reactions [29–32]. In recent years, there have been more and more researches on DBD plasma synthesis of ammonia. For example, Hong et al. [13] synthesized ammonia in a DBD reactor filled with MgO, and the H_2 conversion rate reached 4.2%. Patil et al. [33] compared the effect of a series of carriers (including γ-Al_2O_3, α-Al_2O_3, MgO, CaO, etc.) on DBD ammonia synthesis. Yin et al. [34] studied the influence of different electrode materials Zn, Al, Cu, Fe, etc. on ammonia synthesis, and found that the order of the influence of electrode materials on ammonia synthesis was Pt > SS > Ag > Fe > Cu > Al > Zn. The output range of ammonia was 0.31–1.46 mmol h^{-1}. Mizushima et al. [35] studied the effect of catalysts loaded with transition metals (Ru, Ni, Pt and Fe) on the DBD plasma synthesis of ammonia. Further researches on plasma ammonia synthesis catalysts revealed that Ru-based, Co-based or Ni-based catalysts have attracted more and more attention. For example, Li et al. [36] developed an efficient route for the preparation of activated carbon supported Ru catalysts with high performance for ammonia synthesis. Kim et al. [37] investigated atmospheric-pressure nonthermal plasma synthesis of ammonia over Ru catalysts. They found that the addition of O_2 during the reaction helped the in-situ regeneration of the deactivated catalyst and was beneficial to the synthesis of NH_3. Wang et al. [31] investigated the importance of the Ni/Al_2O_3 catalysts surface on the reaction mechanism. They found that metal sites and weak acidic sites could enhance the production of NH_3 via formation of NH_2 intermediates on the surface. Shah et al. [16] found the Ni-MOF-74 catalysts has a rich pore structure, which improved mass transfer of active particle and product molecules during reaction. And the presence of unsaturated Ni metal sites caused the increase of ammonia production. Hu et al. [38] compared the M/AC (M=Ru, Co, Ni, and Fe) catalysts. The doping of metal on active carbon (AC) improved the reaction performance by up to 37.3%. Compared with Ru-based catalyst, Co- or Ni-based catalyst is relatively common and cheap. Their synergistic effect with plasma is worthy of systematic study.

In this study, ammonia synthesis was carried out in DBD reactors packed with different catalysts, and the effects of N_2/H_2 volume ratio, total gas flow rate, discharge power and discharge temperature on NH_3 yield have been studied. And online plasma diagnosis

combined with N_2 physical adsorption measurement, X-ray diffraction (XRD), high-resolution transmission electron microscopy (HRTEM), NH_3 temperature programmed desorption (NH_3-TPD) and other technologies were used for the characterization and analysis of plasma synergistic catalysis.

Experimental

Experimental Setup

The schematic of the experimental set-up is shown in Fig. 1. A packed-bed DBD reactor was designed for the experiments. The stainless steel rod was used as the high-voltage electrode, connected to the power supply (CTP-2000 K, 40 kHz, Nanjing Suman Electronics Co Ltd, Nanjing, China), and the stainless steel mesh was used as the ground electrode which was wound on the outer wall of the quartz. The length of the discharge quartz tube was 80 mm, and the discharge gap was 2 mm. 2 g of catalyst was filled between the quartz tube and the stainless steel rod, and the DBD reactor was heated by a tube furnace. A mixture of N_2 and H_2 was introduced into the packed-bed DBD plasma reactor, with their volume ratio regulated through the flow meters. By applying a high AC voltage, intense discharge plasma could be generated around the contact points of the catalyst particles. Thus, the NH_3 synthesis reactions would take place under atmospheric pressure.

The charge–voltage (Q–U) Lissajous figure method was used to calculate the discharge power of the packed-bed DBD reactor [36]. The voltage (U) was measured by a high voltage probe (Tektronix, P5100A), the current was measured by a current monitor (Tektronix, ZP1025S), and the electrical signal was collected by a digital oscilloscope (Tektronix, DPO 4104). The capacitance *C* of the capacitor was 0.47 μF, which can be used to determine the amount of charge accumulated in the DBD. The time average optical imaging was

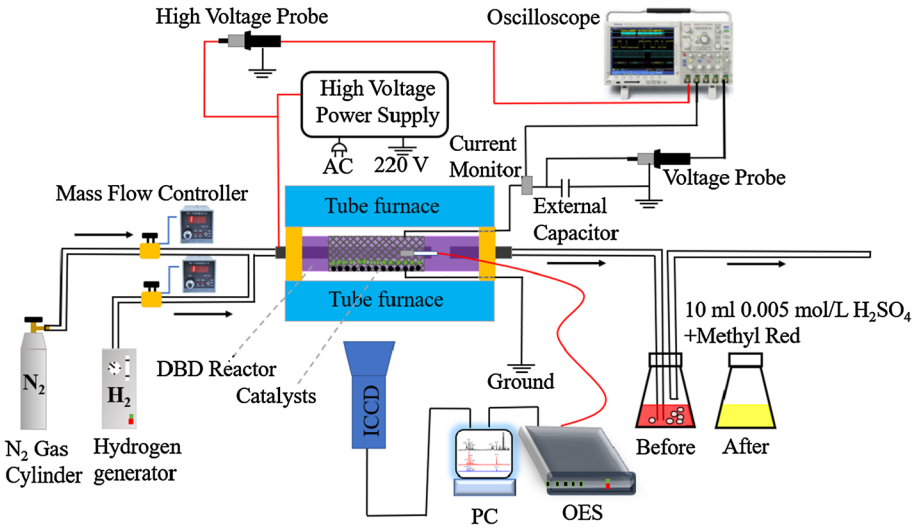

Fig. 1 The experimental setup used for plasma catalytic synthesis of NH_3

measured by an ICCD camera (Princeton Instruments MAX2, 1024 × 1024 pixel), and the exposure time was set to 100 ms to observe the plasma discharge image.

Catalyst Preparation and Characterization

Catalyst prepared by impregnation method is often used in the reaction of plasma synergistic catalysis [31, 36, 38]. 5 wt.% M/Al_2O_3 (M=Ni, Co, Co–Ni) catalysts were prepared by incipient wetness impregnation using nitrate salts (J&K Scientific, 99%) as metal precursor. Al_2O_3 catalyst support (6 g) was added to the solution of nitrate salts. The slurry was continuously stirred at 50 °C for 2 h and aged overnight at room temperature. The samples were then dried at 110 °C for 56 h and calcined at 500 °C for 5 h. And then these sample were reduced at 500 °C under Ar/H_2 mixed atmosphere (100 mL min^{-1}, Ar/H_2 = 7:3) for 5 h. These reduced catalysts were called "fresh catalysts".

Thermogravimetry analysis (TG) was used to determine the optimal calcination temperature of precursors ($Ni(NO_3)_2{\cdot}6H_2O$, $Co(NO_3)_2{\cdot}6H_2O$). The thermogravimetric analysis was performed using a thermogravimetric analyzer (Etelux, Lab2000). Nitrogen with a flow rate of 30 mL min^{-1} was used as the carrier gas. The measurements were carried out from room temperature to 750 °C at a heating rate of 3 °C min^{-1}. The TG curve was given in Fig. S1. The X-ray diffraction (XRD) was used to analyze the crystal structures of the catalysts. The XRD analysis of the catalysts was performed by using a Cu-Kα radiation. The scanning was conducted in the 2θ range of 30°–90° at 6° min^{-1} with a step size of 0.02°. A transmission electron microscope (TEM, Japan, JEM1200EX) was used to perform high-resolution transmission electron microscopy (HRTEM) analysis on the fresh catalyst at an accelerating voltage of 300 kV. Samples were ultrasonic treatment before measurement.

N_2 adsorption–desorption analysis can be used to characterize the physicochemical properties and structural characteristics of the catalysts. Micromeritics ASAP 2460 physical adsorption instrument was used to test the N_2 adsorption–desorption characterization. The specific surface area of the catalyst was calculated according to the Brunauere–Emmette–Teller (BET) equation. The pore size distribution of the catalyst was obtained by the Barrette–Joynere–Halenda (BJH) method. All the catalysts were pretreated at 300 ℃ under vacuum to remove any impurities from the surface.

The surface acidity of the catalysts was evaluated by temperature programmed desorption of ammonia (NH_3-TPD) using a DAS-7000 instrument equipped with a mass analyzer. The fresh catalysts (100 mg) was pretreated and flushed in pure He at 500 °C for 1 h and then cooled down to 50 °C. The adsorption of NH_3 was conducted at 50 °C in a NH_3/He (5 vol.%) gas stream (30 ml min^{-1}) until reaching the adsorption equilibrium. The physical adsorbed NH_3 was removed by pure He (50 ml min^{-1}) at 100 °C. The non-isothermal desorption of NH_3 was performed in pure He at a heating rate of 10 °C min^{-1} in the temperature range of 50–700 °C.

Calculation of Parameters

The chemical titration method was used to quantify the concentration of synthetic ammonia which was introduced into a 10 mL, 0.005 mol L^{-1} dilute H_2SO_4 solution with methyl red indicator to monitor the reaction endpoint. When the color of the solution changed from red to yellow, the H_2SO_4 in the solution was completely neutralized by synthetic NH_3.

Thus, the concentration of synthetic ammonia can be calculated based on the amount of the H_2SO_4. The ammonia mass yield (g s^{-1}) could be calculated from Eq. 1:

$$NH_3 \text{mass yield}\left(\text{g s}^{-1}\right) = \frac{0.005\left(\text{mol L}^{-1}\right) \times 2 \times 10(\text{mL}) \times 17\left(\text{g mol}^{-1}\right)}{t(s) \times 1000\left(\text{mL L}^{-1}\right)} \quad (1)$$

According to the chemical reaction formula: $2NH_3{\cdot}H_2O + H_2SO_4 = (NH_4)_2SO_4 + 2H_2O$, the time ($t$) of indicator changed color meant the 10 mL 0.005 mol L^{-1} H_2SO_4 had been consumed by 100 μmol $NH_3{\cdot}H_2O$. And the ammonia synthesis rate (μmol g^{-1} h^{-1}) could be calculated from Eq. 2:

$$NH_3 \text{ synthesis rate } \left(\mu\text{mol g}^{-1}\text{ h}^{-1}\right) = \frac{\frac{100\ (\mu\text{mol})}{t\ (s)} \times 3600\ \left(s\ \text{h}^{-1}\right)}{m\ (g)} \quad (2)$$

The energy efficiency (g kWh^{-1}) was determined by Eq. 3:

$$E_{NH_3}\left(\text{g kW}h^{-1}\right) = \frac{\text{ammonia mass yield (mg h}^{-1})}{\text{P (W)}} \quad (3)$$

Results and Discussion

Catalyst Characterization

XRD patterns of the fresh catalysts and spent catalysts are shown in Fig. S2. Three major peaks centered at 2θ = 37.6°, 45.9° and 67.0° were identified in the diffraction pattern of pure Al_2O_3, corresponding to the cubic structure of crystalline Al_2O_3 (JCPDS 06-0696). These peaks were also found in the diffraction pattern of the M/Al_2O_3 catalysts. In addition, the peaks of metallic Ni (JCPDS 45-1027) and Co (JCPDS 89-7094) also appeared in the diffraction pattern of the M/Al_2O_3 catalysts. This indicates that the active component has been successfully loaded on Al_2O_3. It is mainly in a metallic state after thermal reduction. Comparing the XRD curves of the catalyst before and after the reaction, it can be seen that the composition of the catalyst has not changed after plasma treatment.

The physical properties of the fresh catalysts measured by N_2 physical adsorption are listed in Table 1. The BET specific surface area of Al_2O_3 was 146 m^2 g^{-1}. The specific surface area of the fresh Al_2O_3-supported metal catalysts increased slightly to between 155 and 164 m^2 g^{-1}. Fresh Al_2O_3 also had the most substantial total pore volume of 0.26 cm^3 g^{-1}, compared to 0.24 cm^3 g^{-1} for the M/Al_2O_3 catalysts. In addition, the average pore

Table 1 Physical characteristics of the fresh catalysts

Samples	Metal loading (wt %)	Surface area (m^2 g^{-1})	Total pore volume (cm^3 g^{-1})	Average pore diameter (nm)
Al_2O_3	–	146	0.26	7.2
Ni/Al_2O_3	5	161	0.24	5.9
Co/Al_2O_3	5	155	0.24	5.9
Co–Ni/Al_2O_3	2.5–2.5	164	0.24	5.8

size of Al_2O_3 was 7.2 nm, and the average pore diameters of $M/A1_2O_3$ were reduced to 5.8–5.9 nm. The increase in the specific surface area of the catalyst may be due to the better dispersion of the supported metal on the support, while the slight decrease of the pore volume and pore diameter of the catalyst may be due to the small amount of supported metal filling the pores of the support. Similar results have been reported in previous studies [39, 40].

The nitrogen adsorption–desorption isotherm of the fresh catalysts are shown in Fig. S3. All samples exhibited type-IV isotherms with H1 hysteresis loops and steep increases in the relative pressure of $0.5 < P/P_o < 0.9$, which indicated that all samples had a mesoporous structure. In addition, when the relative pressure (P/P_o) was 0, as shown in the Fig. S3a–d, it had a higher N_2 adsorption capacity (about 20 $cm^3\ g^{-1}$), which indicated that the catalyst also had a microporous structure [31, 41, 42].

Figure 2 shows the surface morphology and particle size distribution of the fresh catalysts observed by using HRTEM. The particle sizes of most metals on the surface of the catalyst were in the range of 2–16 nm, while the surfaces of Ni/Al_2O_3 and Co/Al_2O_3 catalysts had larger particles with a size of more than 26 nm. Compared with Ni/Al_2O_3 and Co/Al_2O_3, the metal particles loaded on the surface of double metals catalyst $Co–Ni/Al_2O_3$ were more evenly distributed on the surface of the carrier.

The surface acidity of the fresh catalysts was determined by NH_3-TPD. Figure 3 shows the chemical desorption peaks of NH_3 at weak acidic sites (180–240 °C), medium acidic sites (260–320 °C) and strong acidic sites (450–600 °C) [43]. For each catalyst, the amounts of ammonia adsorbed on these locations are listed in Table 2. Obviously, loading the $A1_2O_3$ carrier with metal will reduce the total number of acidic sites (A_{total}), and the order of acidic sites was: Al_2O_3 (0.85 mmol g^{-1}) > Co/Al_2O_3 (0.79 mmol g^{-1}) > $Co–Ni/Al_2O_3$ (0.77 mmol g^{-1}) > Ni/Al_2O_3 (0.71 mmol g^{-1}). Moreover, the concentrations of medium acidic sites and strong acidic sites were significantly reduced after the metal was loaded, which reduces the adsorption energy of the catalyst surface and facilitates the desorption of the product NH_3 from the catalyst surface. This is consistent with the ammonia synthesis rate [31].

Parameters Optimization for DBD Plasma Synthesis of Ammonia

The Effect of N_2/H_2 Volume Ratio on the Ammonia Synthesis Rate

As shown in Fig. 4, the volume ratio of N_2/H_2 under different catalytic conditions had a significant effect on the ammonia synthesis rate. The best $V_{N2/H2}$ was 1:1 in all of the different reaction systems. Compared with the plasma synthesis of ammonia without catalyst, the ammonia synthesis rate was obviously increased after catalyst was filled. The results showed that a sufficient N_2 atmosphere was beneficial to increase the ammonia synthesis rate, because the N–N bond energy in the N_2 molecule is much higher than the H–H bond energy in the H_2 molecule, so more energy is required to break the N–N bond. It is worth noting that different researchers have observed different optimal N_2/H_2 ratios. Hong et al. [20] proposed that this is because the optimal ratio is sensitive to the reduced electric field and the electron density in the reactor.

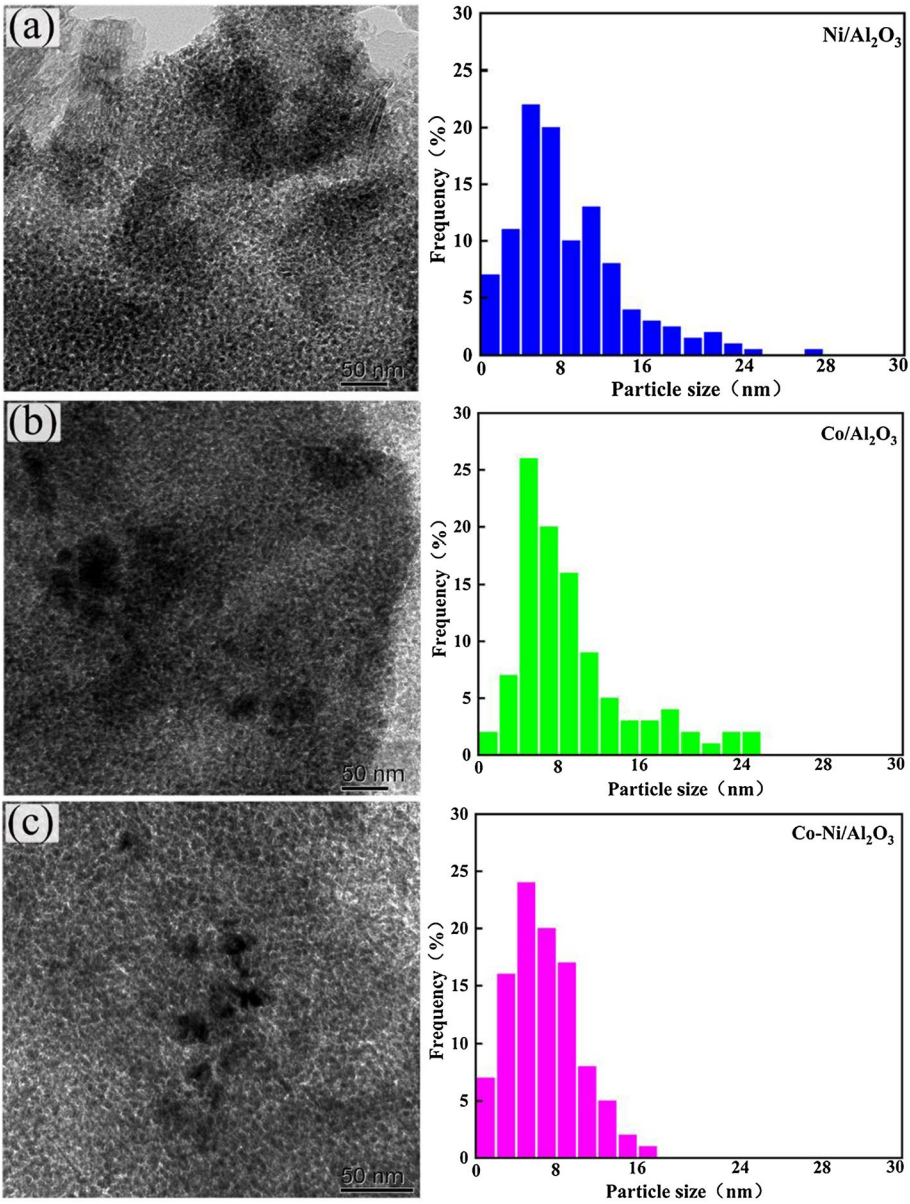

Fig. 2 HRTEM images with the distribution of the particle size (0–30 nm) of the fresh catalysts after reduction: **a** Ni/Al_2O_3, **b** Co/Al_2O_3 and **c** $Co–Ni/Al_2O_3$

The Effect of Total Gas Flow Rate on the Ammonia Synthesis Rate

The ammonia production rate is also related to the reaction gas flow rate. As shown in Fig. 5, the ammonia synthesis rate increased with the increase of total gas flow rate. However, when the total gas flow rate exceeded 120 mL min^{-1}, the growth rate of the ammonia

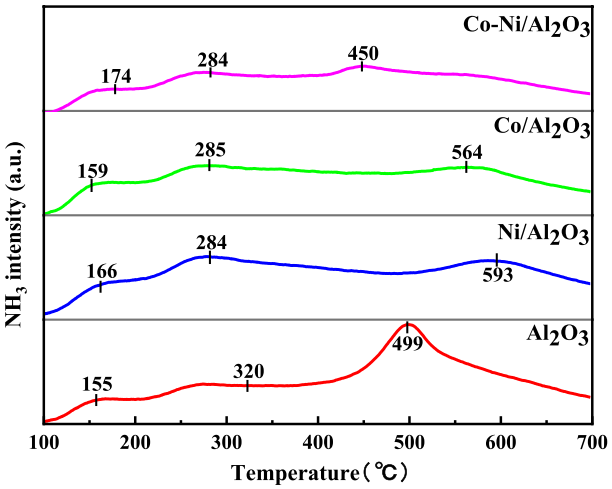

Fig. 3 NH_3-TPD profiles of the fresh catalysts

Table 2 Surface acidity of the fresh catalysts

Catalyst	A_{weak} [a] (mmol g^{-1})	A_{medium} [b] (mmol g^{-1})	A_{total} [c] (mmol g^{-1})
Al_2O_3	0.03	0.31	0.85
Ni/Al_2O_3	0.59	0.11	0.71
Co/Al_2O_3	0.58	0.21	0.79
$Co–Ni/Al_2O_3$	0.42	0.22	0.77

a A_{weak} is the concentration of weak acidic sites;

b A_{medium} is the concentration of medium + strong acidic sites;

c A_{total} is the concentration of acidic sites on the catalyst surface

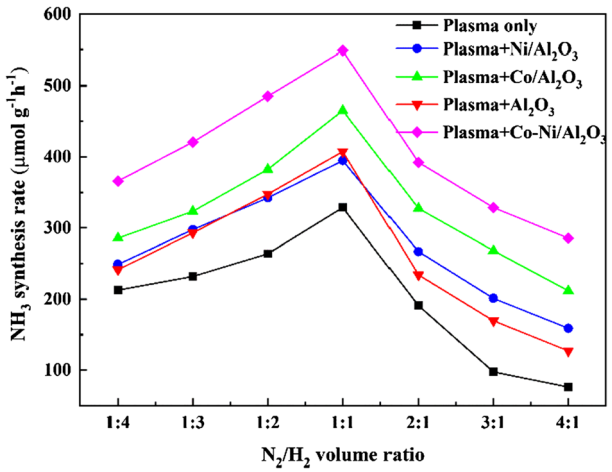

Fig. 4 Effect of N_2/H_2 volume ratio on NH_3 synthesis rate

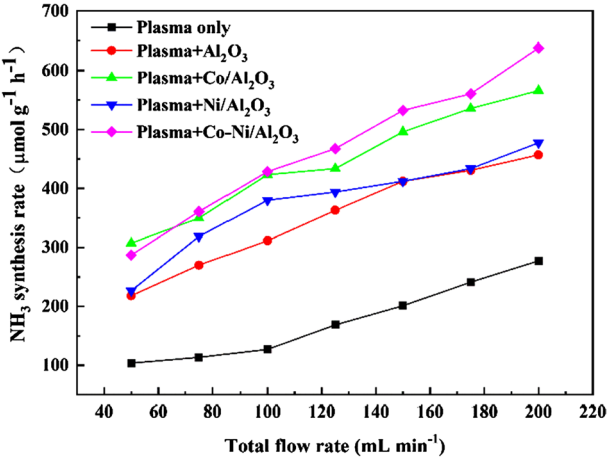

Fig. 5 Effect of total gas flow rate on NH_3 synthesis rate

synthesis rate slowed down. The production rate of ammonia can be determined by the balance difference between ammonia synthesis and loss reactions in the DBD plasma catalytic reaction system. On the one hand, when the pressure is constant, the increase in gas flow rate will provide more raw reactant gas at the same time, increasing the collision probability between reactive particles in the system, which is beneficial to the production of ammonia. However, on the other hand, the increase of the gas flow rate will reduce the residence time of the reactive particles in the reaction system, and some of the active particles will be blown out of the reaction system before they can react. The loss of active particles is not conducive to the production of ammonia. Bai et al. had similar reports [44].

The Effect of Discharge Power on the Ammonia Synthesis Rate

The discharge power is an important parameter for plasma intensified chemical reaction process. The effect of the discharge power on the ammonia synthesis rate under different catalytic conditions is shown in Fig. 6. Obviously, whether or not the catalyst was filled,

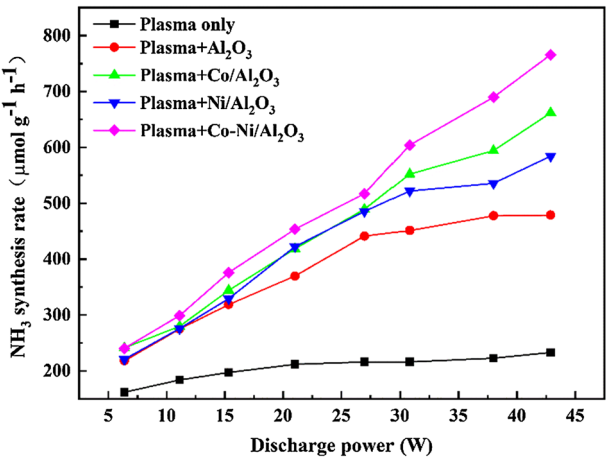

Fig. 6 Effect of discharge power on NH_3 synthesis rate

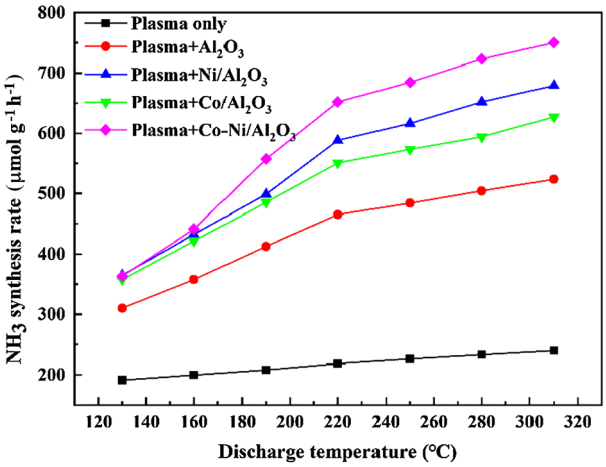

Fig. 7 Effect of discharge temperature on NH_3 synthesis rate

the ammonia synthesis rate of plasma increased with the increase of power. As we all know, increasing the discharge power will strengthen the excitation and ionization of the reactants, which is beneficial to the production of more high-energy electrons and active species [29]. It can increase the number density of reactive species such as N, H and NH_x radicals, thereby improving the reaction performance of plasma catalytic synthesis of NH_3 [44, 45].

The Effect of Discharge Temperature on the Ammonia Synthesis Rate

The ammonia synthesis reaction is an exothermic process, but due to the high stability of N_2 molecule, the industrial ammonia synthesis is mainly carried out at high temperatures. Compared with the conventional Haber–Bosch process, the application of plasma technology can significantly reduce the ammonia synthesis temperature and make the reaction under milder conditions. The effect of discharge temperature on the ammonia synthesis rate under different catalytic conditions is shown in Fig. 7. The discharge temperature had little effect on the ammonia synthesis rate without catalyst. The synthesis rate of NH_3 increased slightly with the increase of temperature. However, after catalysts were filled, the discharge temperature had a significant effect on the NH_3 synthesis rate which increased significantly with the increase of the discharge temperature. N_2 and H_2 molecules in the gas phase collide with electrons to generate nitrogen and hydrogen free radicals, metastable N_2, N_2^+ and H_2^+ particles, which collide with each other to form the intermediate NH_X (X = 1, 2) for ammonia synthesis and the final product NH_3 [46]. However, if the synthesized ammonia is not desorbed from the surface of the catalyst in time, it will be decomposed, thereby reducing the rate of ammonia synthesis. It is difficult to get desorbed at lower temperature, especially for that adsorbed on the pore channel of the catalyst. Increasing the temperature is beneficial to the desorption of the generated ammonia gas from the surface of the catalyst. At the same time, when the catalysts with less acidic sites and strong desorption capacity for NH_3 are applied, this phenomenon are more obvious. There have similar conclusions with previous studies [24].

The stability of catalyst was assessed by continuous reaction for 6 h with different catalysts under same conditions (N_2/H_2 volume ratio was 1:1, total gas flow rate was

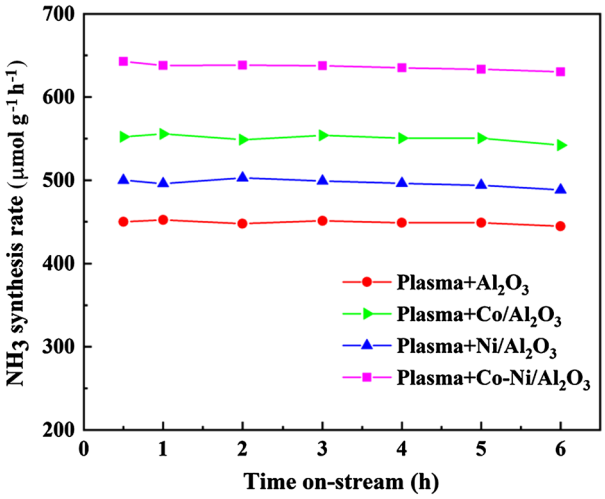

Fig. 8 Stability of different ammonia synthesis catalysts

200 mL min^{-1}, input power was 30.81 W, temperature was 200 °C). The ammonia synthesis rates were recorded per 1 h. The catalysts stability curves are shown in Fig. 8. It was found that all catalysts showed stable performance in whole the 6 h reaction process without deactivation.

The balance between the energy efficiency of the plasma catalysis reaction and the ammonia synthesis rate is of guiding significance for the further development of this technology. Table 3 compares the ammonia synthesis rate and energy efficiency of plasma synthesis of ammonia under different catalytic conditions based on the references and present work. It can be seen that different reaction systems, catalytic systems and process parameters had significant effects on the ammonia synthesis rate. Compared with other plasma-catalyst synergistic synthesis systems, alumina-supported double metals catalyst Co–Ni/$A1_2O_3$ in present work had the best catalytic performance, 3000 μmol h^{-1} of the ammonia yield with 0.83 g kWh^{-1} of energy efficiency. Among the previous work, Peng et al. [24] used Ru-MCM-41 as catalyst for plasma catalytic synthesis of ammonia. Its energy efficiency was 1.7 g kWh^{-1}. The total gas flow rate during their reaction was as high as 4000 mL min^{-1}. However, it was only 200 mL min^{-1} in present work. Shah et al. [16] reported the maximum ammonia yield was 1270 μmol h^{-1} with a very low energy efficiency of only 0.23 g kWh^{-1}. Therefore, higher ammonia yield and energy efficiency can be achieved under milder conditions by packing Co–Ni/$A1_2O_3$ catalyst into DBD plasma reactor in present experimental system.

As we all know, the traditional ammonia synthesis process, Haber–Bosch process, has a conversion rate of 10–15% [47] and an energy efficiency of 100 g kWh^{-1} [48]. Some researchers have conducted a full life cycle assessment for comprehensively compared the conventional NH_3 synthesis process and DBD plasma NH_3 conversion process. It can be seen that current plasma catalytic ammonia synthesis in the conversion rate, energy efficiency and full life cycle assessment also shows the problem of low ammonia synthesis rate and high energy consumption [49, 50]. In order to improve the ammonia production rate and energy efficiency, there are currently many key technical problems need to be solved, such as screening and preparing a stable, efficient, long-life, and low-cost catalyst, designing and optimizing plasma source, using renewable

Table 3 Comparison of synthesis rate and energy efficiency over Co–Ni-based catalysts for plasma intensified ammonia synthesis process

No	Plasma type	Year	Catalyst type	N_2/H_2 volume ratio	Flow rate (mL min^{-1})	Electrical parameters	NH_3 yield[a, b]	Energy efficiency[c] (g kWh^{-1})	Ref
1	DBD	2007	Ni/Al_2O_3 membrane	1:3	30	4.5 kV	1620 μmol h^{-1}	0.18	[35]
2	DBD	2017	$Ni/SiO_2 + BaTiO_3$ (8 g/165 g)	1:3	25	195 W	1071 μmol h^{-1}	0.57	[52]
3	RF plasma	2019	Ni–MOF-74 (200 mg)	–	–	300 W	1270 μmol h^{-1}	0.23	[16]
4	RF plasma	2018	Gold Mesh	1:4	20	300 W	19.1%	0.19	[53]
5	Pulsed-DBD	2017	$Mg–Ru/Al_2O_3$ (17.1 g)	4:1	2000	11,000 W	800 μmol h^{-1}	33.5	[46]
6	Microwave	2008	No Catalyst	–	100	1100 W	0.00025%	0.03	[54]
7	DBD	2017	Ru–MCM-41	1:1	4000	5000 V 26,000 Hz	0.1%	1.7	[24]
8	DBD	2015	$BaTiO_3$/PZT	1:1	38.3	3000 V 500 Hz	2.75%	0.9	[22]
9	DBD	2021	$Co–Ni/Al_2O_3$ (2 g)	1:1	200	30.81 W	3000 μmol h^{-1}	0.83	This work
10	DBD	2021	No Catalyst	1:1	200	20 W	328 μmol h^{-1}	0.86	This work
11	DBD	2021	Al_2O_3 (2 g)	1:1	200	20 W	870 μmol h^{-1}	1.16	This work
12	DBD	2021	$Co–Ni/Al_2O_3$ (2 g)	1:1	200	20 W	960 μmol h^{-1}	1.28	This work

a This was defined as NH3 synthesis rate (μmol g^{-1} h^{-1})*m_c (g) = (μmol h^{-1})

b m_c is the amount of the catalysts used

c The Haber–Bosch (H–B) process for industrial synthesis of ammonia has an energy efficiency of 100 g kWh^{-1}

wind and solar energy and in-depth exploring the mechanism of plasma technology for ammonia synthesis. And previous studies have pointed out that the energy efficiency of ammonia synthesis can be significantly improved by expanding the plasma catalytic system [46, 51]. Therefore, in the future, it is recommended to continue to strengthen the systematic research of important parameters, such as plasma source, reactor, catalyst, and comprehensive consideration of process parameters and energy consumption optimization in the industrialization process.

Characterization of Catalysts Packed Plasma Discharge

Figure 9 shows the ICCD images of plasma discharge under different reaction conditions. Figure 9a shows that the plasma discharge was weak in reaction area without any catalyst. When Al_2O_3 was packed into the reaction area, the plasma discharge was enhanced obviously, as shown in Fig. 9b. The Al_2O_3 supported metal catalysts packed into the discharge gap made this tendency more obviously. The plasma discharge were further enhanced as the Al_2O_3 supported metal catalysts (M/Al_2O_3, M=Co, Ni, Co–Ni) were packed into the discharge gap, as shown in the Fig. 9c–e. The filamentary discharge in the reactor will be transformed into a combination of filamentary discharge and surface discharge in the presence of catalyst [39, 55]. The active particles formed by plasma discharge can interact with the surface of the catalyst. An enhanced electric field was generated near the contact point of the catalyst, which helps the formation of ammonia intermediates, and the surface reaction of the catalyst was increased. which had been well demonstrated in both experimental and modeling studies of packed bed DBD reactors [56, 57]. This conclusion was coincident with the order of the NH_3 synthesis rate with different catalysts: $Co–Ni/Al_2O_3 > Co/Al_2O_3 > Ni/Al_2O_3 > Al_2O_3 >$ only plasma.

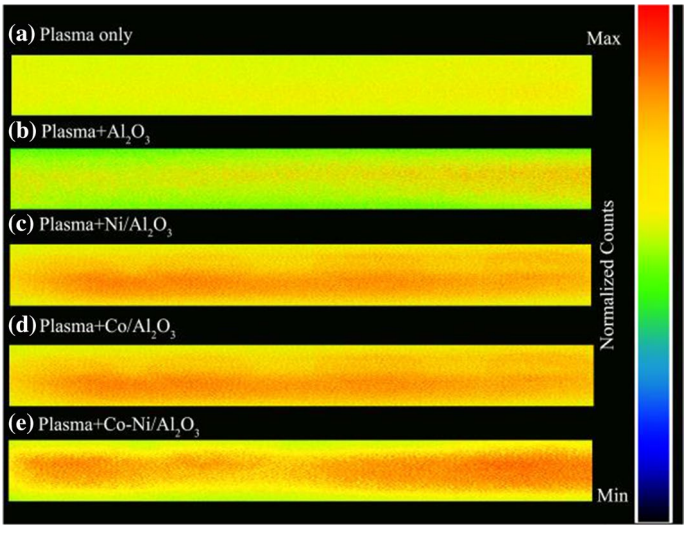

Fig. 9 ICCD camera images of **a** only plasma discharge, **b–e** packed with Al_2O_3, Ni/Al_2O_3, Co/Al_2O_3, $Co–Ni/Al_2O_3$ images with plasma discharge

Table 4 Discharge characteristics under different catalytic conditions

	E (kV cm^{-1})	Input power (W)	Output power (W)	Power efficiency (%)
Plasma only	8.15	48	26.38	54.96
Al_2O_3	10.9	48	27.03	56.31
Ni/Al_2O_3	11.9	48	28.37	59.10
Co/Al_2O_3	13.1	48	28.58	59.54
$Co–Ni/Al_2O_3$	14.0	48	30.81	64.19

In order to further understand the discharge characteristics under different catalytic conditions, plasma electrical diagnosis was carried out. Figure S4 shows the U–Q Lissajous diagram under different catalytic conditions measured by an oscilloscope. And the detailed discharge characteristics has been calculated and listed in Table 4 (The calculation method can be found in section II of the Supporting Information). The average electric field (E) increased after filling the catalysts into the discharge area. This may be due to the increase of the dielectric constant of the filling material, the polarization of the contact point, and the deposition of charge [58, 59]. The improvement order of power efficiency after packing catalyst was: $Co–Ni/Al_2O_3 > Co/Al_2O_3 > Ni/Al_2O_3 > Al_2O_3 >$ plasma only, which was coincident with the change of the electric field. At the same time, it was also agreed with the order of the NH_3 synthesis rate with different catalysts.

Conclusions

In this paper, a coaxial packed-bed DBD reactor has been developed for plasma catalytic synthesis of NH_3. The Al_2O_3 supported transition metals M/Al_2O_3 (M = Co, Ni, Co–Ni) were used as catalyst in the plasma synthesis reaction. The influences of reaction conditions on the NH_3 synthesis rate were explored. Compared with only plasma discharge to synthesize ammonia, plasma assisted catalysis significantly improved the ammonia synthesis rate and energy efficiency. The order of ammonia synthesis rate and energy efficiency was: $Co–Ni/Al_2O_3 > Co/Al_2O_3 > Ni/Al_2O_3 > Al_2O_3 >$ plasma only. The catalysts can maintain stability for at least 6 h. The investigation of process parameters found that the best N_2/H_2 volume ratio under different catalytic conditions was 1:1. In addition, increasing the total gas flow rate, discharge power or reaction temperature was beneficial to improve the NH_3 synthesis rate. The highest NH_3 synthesis rate was 1500 μmol g^{-1} h^{-1} by using Al_2O_3 supported double metal catalyst $Co–Ni/Al_2O_3$. $Co–Ni/Al_2O_3$ bimetal catalyst not only has the advantage of lower price, but also plays a role in reducing the acidity of the catalyst surface and enhancing the plasma discharge, which is beneficial to the synthesis of ammonia.

Supplementary Information The online version contains supplementary material available at https://doi.org/10.1007/s11090-021-10223-1.

Acknowledgements This work was supported by National Natural Science Foundation of China (No. 11505013, 11875090), Beijing Municipal Natural Science Foundation (No. 1192008) and Science and Technology Project of Beijing Municipal Education Commission (No. KM202010015003).

References

1. Galloway JN, Townsend AR, Erisman JW, Bekunda M, Cai ZC, Freney JR, Martinelli LA, Seitzinger SP, Sutton MA (2008) Science 320:889–892
2. Licht S, Cui B, Wang B, Li FF, Lau J, Liu S (2014) Science 345:637–640
3. Valera-Medina A, Xiao H, Owen-Jones M, David WIF, Bowen PJ (2018) Prog Energy Combust Sci 69:63–102
4. Dunn R, Lovegrove K, Burgess G (2012) Proc IEEE 100:391–400
5. Chen C, Zhao LL, Lavine AS (2018) Sol Energy 176:638–647
6. Avery WH (1988) Int J Hydrogen Energy 13:761–773
7. Morgan E, Manwell J, McGowan J (2014) Renewable Energy 72:51–61
8. Yapicioglu A, Dincer I (2019) Renewable Sustainable Energy Rev 103:96–108
9. Hargreaves JSJ (2014) Appl Petrochem Res 4:3–10
10. Aika K-i (1972) Hori H, Ozaki A. J Catal 27:424–431
11. Tanabe Y, Nishibayashi Y (2013) Coord Chem Rev 257:2551–2564
12. Marnellos G, Stoukides M (1998) Science 282:98–100
13. Hong J, Pancheshnyi S, Tam E, Lowke JJ, Prawer S, Murphy AB (2018) J Phys D: Appl Phys 51: 109501
14. Kitano M, Inoue Y, Yamazaki Y, Hayashi F, Kanbara S, Matsuishi S, Yokoyama T, Kim SW, Hara M, Hosono H (2012) Nat Chem 4:934–940
15. Mehta P, Barboun P, Herrera FA, Kim J, Rumbach P, Go DB, Hicks JC, Schneider WF (2018) Nat Catal 1:269–275
16. Shah J, Wu T, Lucero J, Carreon MA, Carreon ML (2018) ACS Sustainable Chem Eng 7:377–383
17. Xie Q, Zhuge S, Song X, Lu M, Ruan R, Nie Y, Ji J (2018) Int J Hydrogen Energy 43:14885–14891
18. Tu X, Whitehead JC (2012) Appl Catal B 125:439–448
19. Xie D, Sun Y, Zhu T, Fan X, Hong X, Yang W (2016) RSC Adv 6:105338–105346
20. Hong J, Aramesh M, Shimoni O, Seo DH, Yick S, Greig A, Charles C, Prawer S, Murphy AB (2016) Plasma Chem Plasma Process 36:917–940
21. Yuan D, Ding C, He Y, Wang Z, Kumar S, Zhu Y, Cen K (2017) Plasma Chem Plasma Process 37:1165–1173
22. Gómez-Ramírez A, Cotrino J, Lambert RM, González-Elipe AR (2015) Plasma Sources Sci Technol 24: 065011
23. Ma H, Chen P, Zhang M, Lin X, Ruan R (2002) Plasma Chem Plasma Process 22(2):239–254
24. Peng P, Cheng Y, Hatzenbeller R, Addy M, Zhou N, Schiappacasse C, Chen D, Zhang Y, Anderson E, Liu Y, Chen P, Ruan R (2017) Int J Hydrogen Energy 42:19056–19066
25. Sheng Z, Watanabe Y, Kim H-H, Yao S, Nozaki T (2020) Chem Eng J 399: 125751
26. Yi Y, Zhang R, Wang L, Yan J, Zhang J, Guo H (2017) ACS Omega 2:9199–9210
27. Wang J, AlQahtani MS, Wang X, Knecht SD, Bilén SG, Song C, Chu W (2021) Green Chem 23:1642–1647
28. Zeng YX, Tu X (2016) IEEE Trans Plasma Sci 44:405–411
29. Neyts EC, Ostrikov K, Sunkara MK, Bogaerts A (2015) Chem Rev 115:13408–13446
30. Wang L, Yi YH, Wu CF, Guo HC, Tu X (2017) Angew Chem Int Ed 56:13679–13683
31. Wang Y, Craven M, Yu X, Ding J, Bryant P, Huang J, Tu X (2019) ACS Catal 9:10780–10793
32. Stere CE, Anderson JA, Chansai S, Delgado JJ, Goguet A, Graham WG, Hardacre C, Taylor SFR, Tu X, Wang Z, Yang H (2017) Angew Chem Int Ed Engl 56:5579–5583
33. Patil BS, van Kaathoven ASR, Peeters FJJ, Cherkasov N, Lang J, Wang Q, Hessel V (2020) J Phys D: Appl Phys 53:144003
34. Yin KS, Venugopalan M (1983) Plasma Chem Plasma Process 3:343–350
35. Mizushima T, Matsumoto K, Ohkita H, Kakuta N (2007) Plasma Chem Plasma Process 27:1–11
36. Li Y, Pan C, Han W, Chai H, Liu H (2011) Catal Today 174(1):97–105
37. Kim HH, Teramoto Y, Ogata A, Takagi H, Nanba T (2017) Plasma Processes Polym 14:1600157
38. Hu X, Zhu X, Wu X, Cai Y, Tu X (2020) Plasma Process Polym 17:2000072
39. Wu J, Zhao Z, Huang T, Sheng P, Zhang H, Tian H, Zhao X, Zhao L, He P, Ren J, Gao K (2017) Catal commun 93:62
40. Serrano-Ruiz JC, Ramos-Ferna´ndez EV, Silvestre-Albero J, Sepu´lveda-Escribano A, Rodrı´guez-Reinoso F (2008) Mater Res Bull 43:1850
41. Peng P, Li Y, Cheng Y, Deng S, Chen P, Ruan R (2016) Plasma Chem Plasma Process 36(5):120110.
42. Kowalczyk Z, Krukowski M, Rarog-Pilecka W, Szmigiel D, Zielinski J (2003) Appl Catal A Gen 248(12):67–73
43. Wang C, Ma X, Ge Q, Xu H (2015) Catal Sci Technol 5:1847–1853

44. Bai MD, Zhang ZT, Bai XY, Bai MD, Ning W (2003) IEEE Trans Plasma Sci 31:1285–1291
45. Uyama H, Matsumoto O (1989) Plasma Chem Plasma Process 9:13
46. Zhu X, Hu X, Wu X, Cai H, Zhang H, Tu X (2020) J Phys D: Appl Phys 53: 164002
47. J Humphreys, Lan R, Tao S (2020) Adv Energy Sustainability Res, 2000043
48. Liu HZ (2011) Chem Ind Eng Pro (China) 30:1147–1157
49. Anastasopoulou A, Keijzer R, Patil B, Lang J, van Rooij G, Hessel V (2020) J Ind Ecol 24:1171–1185
50. Riotto T, Cao G, Luyben WL, Baltrusaitis J (2021) ACS Sustain Chem Eng 9:13233–13244
51. Bai MD, Bai XY, Zhang ZT, Bai MD (2000) Plasma Chem Plasma Process 20:511–520
52. Akay G, Zhang K (2017) Ind Eng Chem Res 56:457–468
53. Shah J, Wang WZ, Bogaerts A, Carreon ML (2018) ACS Appl Energy Mater 1:4824–4839
54. Nakajima J, Sekiguchi H (2008) Thin Solid Films 516:4446–4451
55. Carrasco E, Jimenez-Redondo M, Tanarro I, Herrero VJ (2011) Phys Chem Chem Phys 13:19561
56. Tu X, Gallon HJ, Whitehead JC (2011) IEEE Trans Plasma Sci 39:2172–2173
57. Gao M, Zhang Y, Wang H, Guo B, Zhang Q, Bogaerts A (2018) Catalysts 8:248
58. Mei DH, Zhu XB, He YL, Yan JD, Tu X (2015) Plasma Sources Sci Technol 24: 015011
59. Van Laer K, Bogaerts A (2016) Plasma Sources Sci Technol 25: 015002